AIAA 99-0600

Shock Structure of a Spherical Projectile in Weakly Ionized Air

Heard Lowry, Chip Stepanek, Les Crosswy,
Peter Sherrouse, Mike Smith, Lin Price,
Wim Ruyten, and John Felderman
Sverdrup Technology, Inc., AEDC Group
Arnold Engineering Development Center
Arnold Air Force Base, Tennessee 37389-4300

19991130 094

37th AIAA Aerospace Sciences Meeting & Exhibit
January 11-14, 1999 / Reno, NV

SHOCK STRUCTURE OF A SPHERICAL PROJECTILE IN WEAKLY IONIZED AIR*

Heard Lowry, Chip Stepanek[†], Les Crosswy, Peter Sherrouse, Mike Smith[‡], Lin Price, Wim Ruyten[†],
and John Felderman
Sverdrup Technology, Inc., AEDC Group
Arnold AFB, TN 37389-4300

Abstract

A test program was undertaken at Arnold Engineering Development Center (AEDC) to investigate previously reported measurements of anomalous shock standoffs in weakly ionized gases by installing an RF plasma generator in AEDC's S1 Hypervelocity Impact Range. The AEDC tests were conducted by firing 9.5- and 19.1- mm-diam spheres in air at velocities in the range 1200 to 1700 m/sec and at pressures in the range 15 to 40 torr. The bow shock shape data were obtained using holographic interferometry techniques. A standoff distance was measured and ratioed to the projectile radius. The data were compared to CFD calculations for a uniform gas temperature. Confirmation of the anomalous shock standoffs was obtained, and efforts were subsequently directed towards separating the effects of ionization from the effects of gas temperature on the shock profile. The temperature was measured by three different techniques (thermocouple, N_2^+ emission spectrum, and NO-PLIF); the results appear to be much lower than necessary to explain the measured shock standoffs by uniform gas effects.

Introduction

A ballistic range with a plasma generator provides an excellent exploratory environment for research insight into the nature of hypersonic flow in weakly ionized gases. Recent tests in AEDC's S1 Hypervelocity Impact Range[1,2]) required the use of diagnostic instrumentation that was not significantly affected by a weakly ionized gas environment. Measurements of the shock boundary and gas temperature were necessary to further investigate previously observed anomalous shock shapes and standoffs[3,4]), where the standoff distance of the bow shock was several times the estimated thermal value. The AEDC tests were conducted at velocities in the range 1200 to 1700 m/sec and at pressures in the range 15 to 40 torr with all shots in an air environment. The projectiles were 9.5- and 19.1- mm-diam metal spheres.

A number of instrumentation systems were used to characterize the plasma, including NO-PLIF and spectroscopy. The bow shock shape data were obtained using focused shadowgraph and holographic interferometry techniques.

Test Facility

Ballistic Range

The projectile launcher of the S1 Hypervelocity Impact Range was configured as a single-stage powder gun. Three multibeam laser detector systems were used to identify the position of the projectile during its flight down the range and produce the proper instrumentation control signals.

Plasma Generator Development

A plasma generator very similar to that of Bedin and Mishin[4] was developed and installed in the range. The plasma region created was nonuniform in nature, with several distinct discharge paths. To facilitate the separation of thermal and ionization effects in the shock standoff measurements, a triggered spark gap was introduced so that the plasma generator electrical discharge could be quickly shut down. The shock structure around the projectile could be recorded at selectable time intervals after the RF power was turned off. In a neutral environment, the shock standoff should only be influenced by the gas temperature. A more complete description of the AEDC plasma generator is given in Ref. 2.

Approved for public release; distribution unlimited.

The plasma generator was operated at the same operating current for these tests, and was limited to a duty cycle of 30 sec on and at least 300 sec off to prevent overheating of the plasma generator electrodes. A visually uniform electrical glow discharge inside the electrode array was desired. However, the actual electrical discharge appeared to consist of a small number of discrete, glowing, anode-to-cathode streamers. Several modifications were made to reduce spurious discharges, arcing, and overheating.

A plan view of the test chamber, plasma generator, and diagnostic equipment is shown in Fig. 1. A more detailed representation of the plasma generator is shown in Fig. 2. A mechanism for traversing Langmuir or thermocouple probes along the length of the plasma generator was provided.

Instrumentation and Results

Probes

Accelerometers were installed at three locations in the range to measure acoustic disturbances during a shot. One was located at the exit of the launch tube so that the vibration from the launch could be recorded and a time trace of the entire activity of the shot from launch to impact could be captured. The other two accelerometers were located as shown in Fig. 1. A microphone was also installed on the top flange to measure the pressure fluctuations in the chamber during the shot. The accelerometer and microphone data indicated no significant acoustic disturbances during a shot which might affect the gas in the plasma region.

Initial temperature measurements were made with an electrically floating metal-sheathed thermocouple, but due to the significant electrical interaction between the probe and the discharge, the data were acquired only after the plasma had been on for a period of time and then shut off. These temperature data are shown in Fig. 3. Uncertainties regarding this data include: (1) the time required for the plasma to come to an equilibrium, (2) the time required for the probe to stabilize, and (3) the influence of the electron density on the probe compared to the effect of gas

temperature. The data indicated a gas temperature of approximately 1000 K.

The metal sheath of this probe was removed, and a high-temperature cement used to electrically isolate the thermocouple junction from the electrical discharge. However, the conductivity of the cement was high enough at the elevated temperatures of the discharge that the probe tip and thermocouple junction were destroyed a few seconds after its immersion. The thermocouple's presence altered the current paths in the plasma,
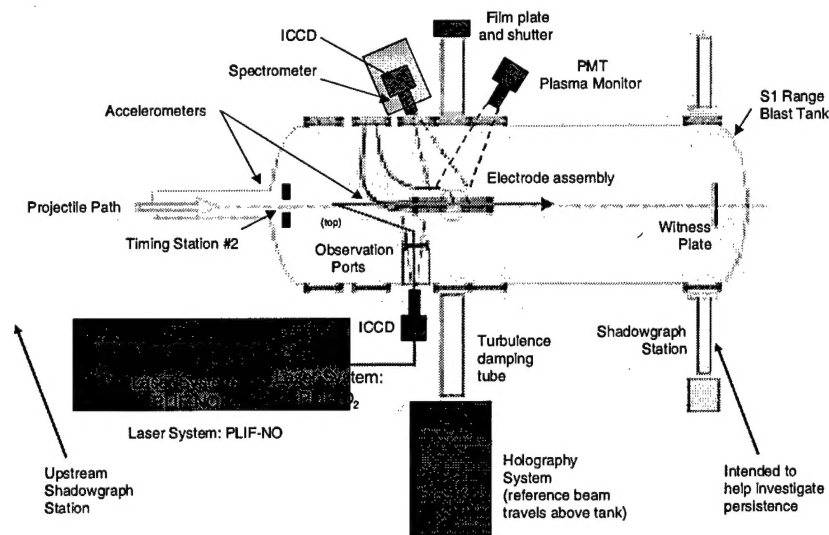

Figure 1. Range instrumentation for plasmadynamic testing.

indicating an attachment of electron flow to the probe through the wires inside the ceramic insulator. A dummy probe with no internal electrical wiring did not show this effect.

A probe with a machinable ceramic tip that did not interact electrically with the discharge, was fabricated, but it exhibited an unfavorable thermal time constant (~ 30 sec). A plasma-spray ceramic coating technique was investigated as a means of providing an insulated thermocouple with a much shorter thermal time constant, but the test probes did not survive the application treatment. The high-temperature cement approach will be attempted using a more complete heat soak to drive off water vapor which might have caused the increased conductivity.

Attempts were made to use single and double Langmuir probes for measurements of the plasma properties, especially electron number density. RF compensation circuit elements[5] were incorporated into the probe circuit designs to counter the effects of RF probe currents induced by interaction of the

2

probe with the RF electrical discharge. Despite these modifications, electrical interaction of the Langmuir probes with the RF electrical discharge was so intense that the tungsten probe tips were burned away and the ammeter output was saturated so that no useful measurements could be made.
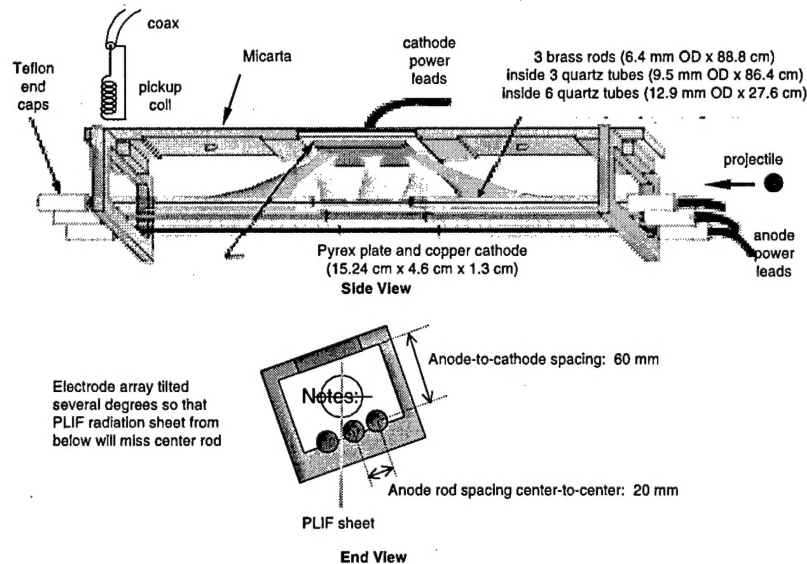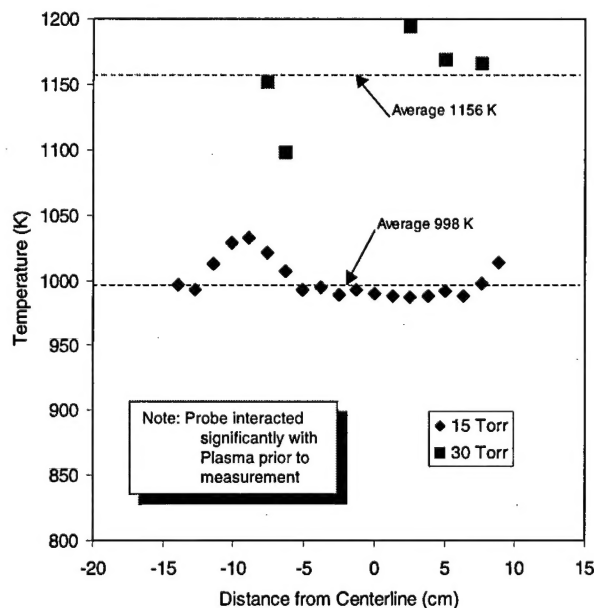

Figure 2. Details of plasma generator.

Figure 3. Thermocouple survey of plasma.

Plasma Monitor

A plasma monitor, which used a photomultiplier tube (PMT), is indicated in Fig. 1. This device is used to record the time history of the intensity of the spatially integrated broadband visible radiation produced by the plasma

generator. From these data the decay, strength, and stability of the radiative processes were examined. An example is shown in Fig. 4. Note that the sinusoidal waveform is evident, even though the signal is derived from a spatial integration over the entire plasma structure. The results of plasma cutoff are shown in Fig. 5, where the output dies off in about 3 μsec. At these projectile speeds the projectile moves approximately 2 mm during one plasma cycle.

Cameras

Imaging of the plasma region with an intensified CCD (ICCD) camera (576 x 384 pixels) provided information on the spatial distribution of NO and other constituents at key times during a shot (only one image per shot), and left a record that could be examined for plasma field disturbances and interactions with the projectile. The camera gate was controlled so that snapshots of the plasma were taken at the same time the projectile passed through the plasma region, as shown in Fig. 6. The gate width was nominally 10 μsec, during which the projectile typically traveled about 1.52 cm. Images were acquired for every shot.
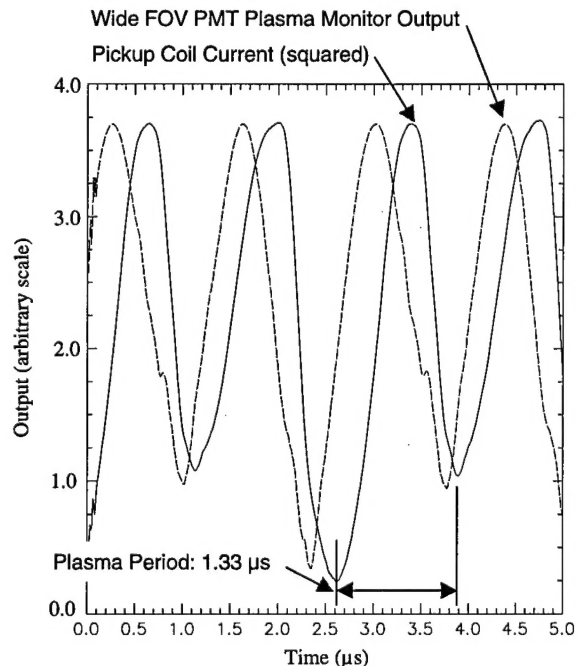

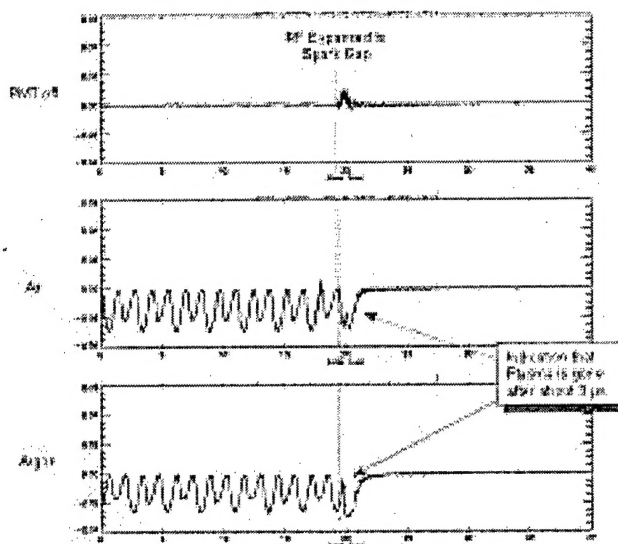**Figure 4.** Typical output of plasma monitor.
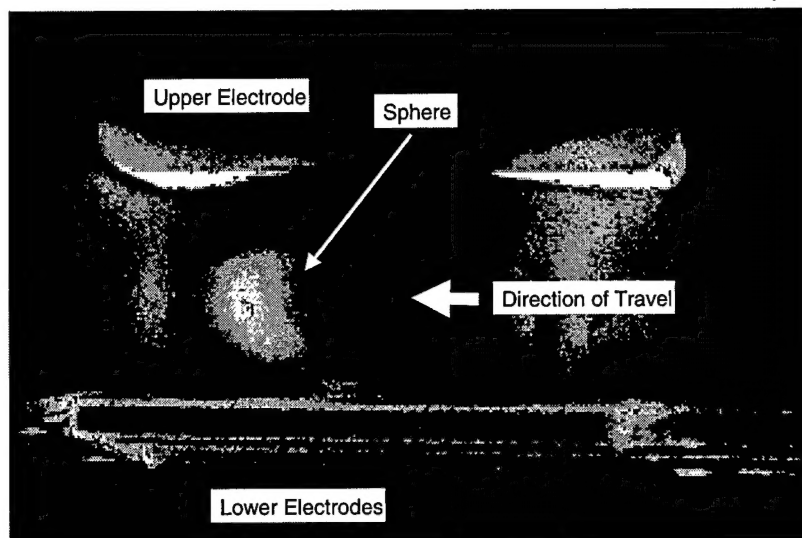
3

Figure 5. Plasma cutoff data.

Figure 6. Emission image of shot 575

shape across the light and dark emission regions. Calculations of the spectral band shape for a range of temperatures were performed so that its temperature sensitivity could be examined. The calculated spectra at different temperatures were not significantly different for this band at gas temperatures in the range 500 – 3500 K. A similar comparison for the (0,3) band will be performed.

PLIF

The high-energy electrons generated in the plasma dissociate a portion of the nitrogen and oxygen in the air, and a considerable amount of nitric oxide (NO) is produced. Planar laser-induced fluorescence (PLIF) is an excellent technique for measuring the global distribution and/or temperature of NO in a flow field[7,8] and has been used previously at AEDC [9,10].

A frequency tripled Nd:YAG laser (355 nm) was used to pump a tunable dye laser whose output was frequency doubled by a BBO crystal to yield a 1-2 mJ pulse at a wavelength of 226 nm with a bandwidth of 1 cm^{-1}. Nitric oxide absorbs in this wavelength region, exciting the NO $A{\leftarrow}X$ $\gamma(0,0)$ band. Wavelength tuning was accomplished by using a UV pulsed wavemeter. The transitions used for the PLIF measurements were the $R_{11}(13)$ 225.716-nm line and the $P_{21}(28)$ 225.134-nm line. These transitions were selected because of the temperature dependence of their absorptive strengths in the range of interest, nominally 1,000 K - 2,000 K, and because of their relative isolation in wavelength from neighboring transitions. Mirrors were installed inside the tank so that the axial profile could be measured.

The resultant NO fluorescence was imaged onto two 2-D ICCD cameras (576 x 384 pixels). A Schott® UG-5 glass filter (175-nm bandwidth centered at 300 nm) was used to eliminate Rayleigh and room light. There was not sufficient laser power in an extended sheet for the PLIF signal to overcome the emission from the plasma, so the 226-nm laser light was formed into pencil beams using a cylindrical lens and passed through the measurement region. The data acquisition, processing, and control of the camera were

Spectroscopy

The temperature of the plasma was investigated by recording spatially resolved emission spectra of the N_2^+ emission with a 0.275-m spectrometer (0.03-nm resolution) with an ICCD camera mounted at the exit plane. The measured intensities of the rotational lines in this spectra compare favorably with reported calculations for a temperature range of 600 - 800 K (Ref. 6), as shown in Fig. 7. A closer examination and comparison of these data to a more extensive set of calculations must be pursued.

The NO spectrum was investigated at various points in the plasma region for the (0,1) vibrational band. The spectra were normalized and overlaid to show that there was minimal variability of the band

accomplished through the use of a 486 PC. A complete description of the data analysis techniques can be found in another paper (Smith, et al., AIAA-99-0721) in this conference.
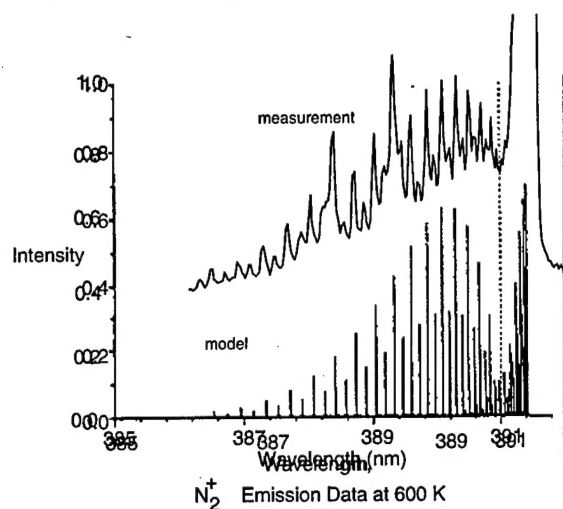

Figure 7. N_2^+ emission spectra.

Preliminary data were acquired on each line at significantly different times. Later, however, another laser system was installed so that the transitions could be pumped nearly simultaneously (within about 700 nsec). The horizontal profile data for each transition are shown in Fig. 8. The temperature profiles are also shown in Fig. 8.

The rotational temperature derived from these measurements is nonuniform along the path of the laser beam (and thus the projectile) and appears to be highest inside the strongest visible features of the plasma, where the excitation temperature is highest. The degree to which the translational, electronic, vibrational, and rotational temperatures are in equilibrium is the difficult question. This technique can be used to quantify spatial temperature variations and provide a temperature map of the plasma volume.

Shock Imaging

Two focused shadowgraph systems were installed to provide shock standoff and shock shape

data in clear air before and after projectile passage through the plasma generator. The downrange system provided data that indicated no significant persistence effect in the anomalous shock standoff.

Holography was selected to visualize the flow structure around the projectile as it encountered the plasma field. The disturbances visualized are the result of localized changes in gas pressure, temperature, and gas optical properties (e.g., indices of refraction and plasma fields). Holography was employed over other techniques for the following reasons: (1) holography allows versatility in the replay to employ, along with interferograms, other techniques with little degradation in image quality; (2) shadowgraph, while being vibration insensitive, is inherently less sensitive to the shock features and has inherently poor focus; (3) Schlieren, while having the potential of high sensitivity, is risky to employ to high-speed single-shot events due to relative motion of the knife edge to the laser beam (a result of system vibration, creep, and pulse-to-pulse spatial repeatability of the laser); (4) Schlieren is only sensitive to gradients perpendicular to the knife edge and is, therefore, limited to one axis of sensitivity per image; and (5) the sensitivity of infinite fringe interferograms is roughly equal to that of a Schlieren system with a perfect optical system and alignment without the need for expensive diffraction-limited optical
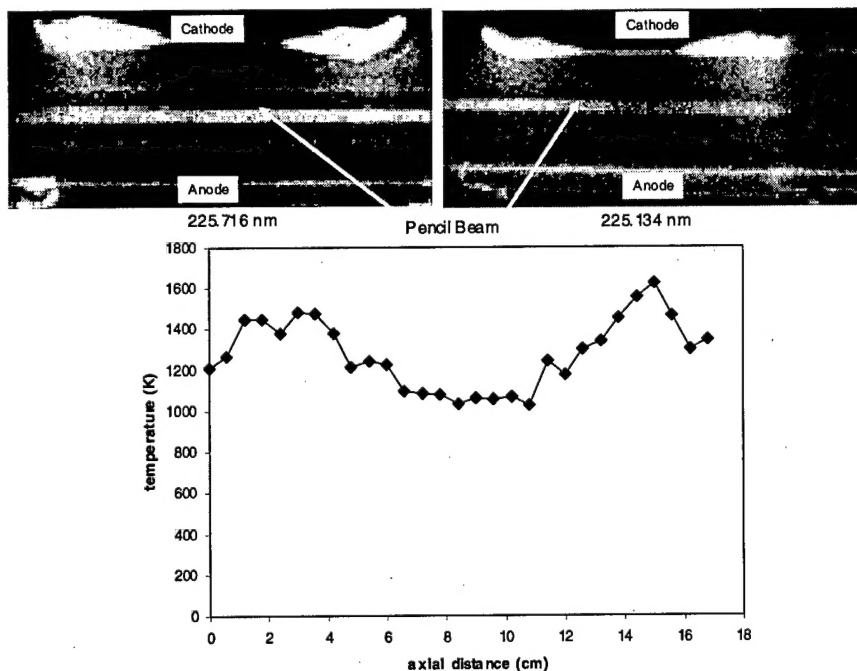

Figure 8. Results of dual LIF in plasma.

components. It should be noted that, with a 30-torr gas pressure in the cell, any of the optical techniques mentioned above are pushed to the limit of sensitivity.

A pulsed ruby laser was used to record a virtual image (absorption type) transmission hologram of the plasma region. The reference beam was created from a portion of the laser output. Under the low-temperature conditions which occur when the plasma is not present, very sharp shock images were obtained in the ballistic range. When the plasma was on, the high-temperature and low-pressure conditions (and possible plasma interaction) yielded very weak shocks that were at the threshold of discrimination. This low contrast had to compete with intensity gradients of the fringes that constitute the interferogram.

Reference holograms obtained with the cell pumped down to the desired pressure and with the plasma on or off, respective of the test configuration to be run were used. The hologram reconstruction system utilized a fixture that provided adjustment for relative motion between the reference and test plates to obtain the "infinite fringe" setting.

Results and Analysis

The holography data from the plasma region, as compared to the focused shadowgraph data upstream and downstream of the plasma region or the holography data with the plasma off, indicate a significant effect of the plasma on the shock structure and shock standoff. A split image of the holography of a shot with and without the plasma is shown in Fig. 9. The standoff distance are significantly larger when the plasma is on. The standoff data is converted to standoff ratio by dividing by the radius of the projectile in an effort to remove the major scale effect.

Shock Shape Fit to Parabola

Plasma On -- The shock shape was analyzed with the assistance of a computer running IDL software in order to reduce the uncertainties associated with a manual digitization process. The set of data points describing the shock profile was fitted to a parabola, as illustrated in Fig. 10. A standoff distance was then measured and ratioed to the projectile radius. An example of the standoff ratio analysis is given in Fig. 11, where 5 rows of the digitized image are overlaid to show the transition areas of the shock and the sphere. A similar example of one of the shots with weaker shock structure is given in Fig. 12.

A set of shock standoff data for plasma on and off conditions was acquired and plotted against AEDC CFD calculations (from Anderson[11]) and the

work of Mishin, et al.[3] in Fig. 13. The extrapolation of the data horizontally to the CFD calculations for the plasma on condition would yield a temperature of greater than 2000 K, as is shown in Fig. 14.
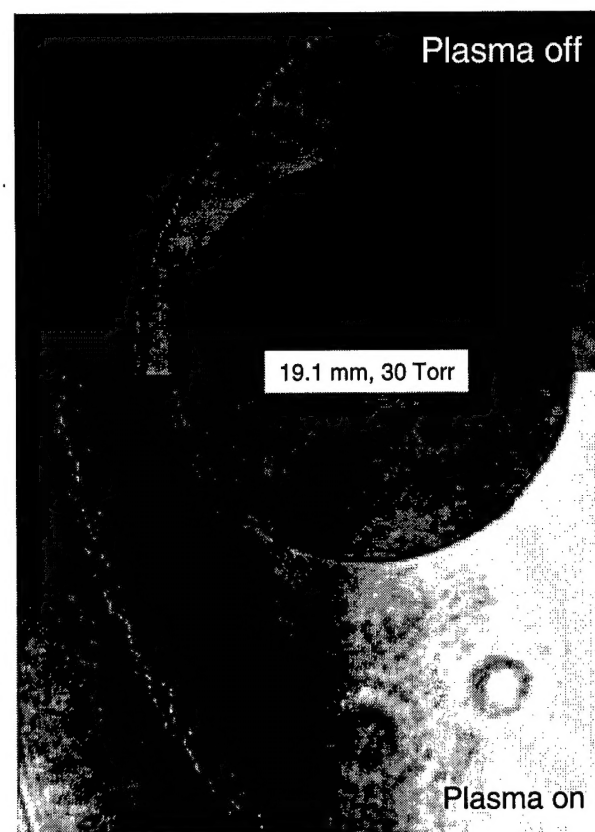

Figure 9. Shock shape comparison.

Plasma Off -- Several shots were made with the plasma cut off at various times before the arrival of the projectile in order to examine the decay of the shock standoff. The data are shown in Fig. 15. If the anomalous shock effect were due primarily to ionization, there would be a rapid drop in the standoff ratio compared to that expected for the gas temperature, which would eventually (~ 50 msec) decrease to ambient. If only temperature effects were involved, there would be no sharp drop, but a gradual decrease. The standoff ratios for the shots where the plasma was off for just a few msec are significantly lower than expected for a purely temperature effect. The shot where the plasma had been off for 100 msec (shot 578) shows clearly that over this length of time the standoff effect had relaxed to that of ambient conditions. More data are needed to fill in portions of this graph so that a more complete idea of the decay function can be established. Buoyancy effects, where the hot gas may pass out of the
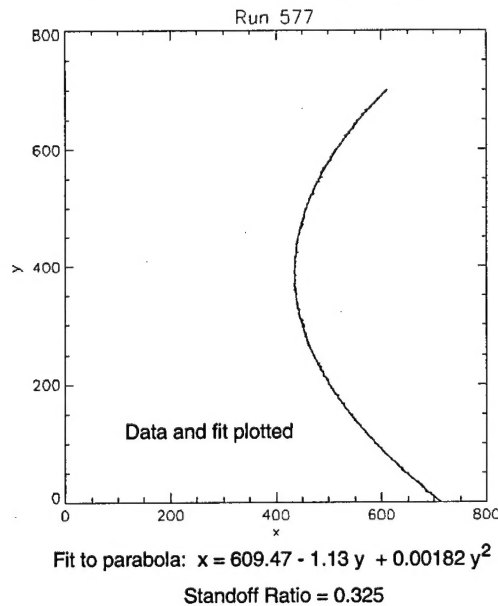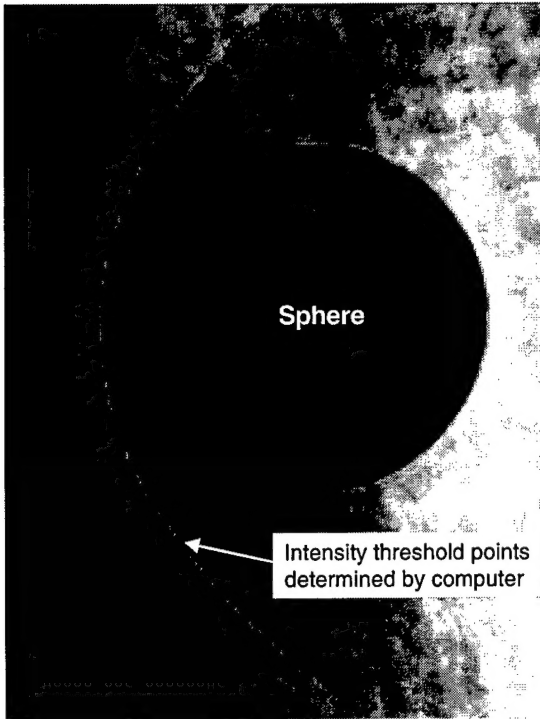
Run 578

Run 577

Fit to parabola: $x = 609.47 - 1.13\,y + 0.00182\,y^2$

Standoff Ratio = 0.325

Figure 10. Computer-aided shock shape analysis.

Figure 11. Cross-section of intensity image (100 msec after plasma cutoff).

measurement region, must also be considered in this analysis.

The curve fits from these shots are plotted in comparison with CFD calculations at three temperatures in Fig. 16 for the 19.1-mm spheres. A similar plot for the 9.5-mm spheres is shown in Fig. 17. Again, it can be seen that the plasma-on condition yields a significantly larger standoff ratio.
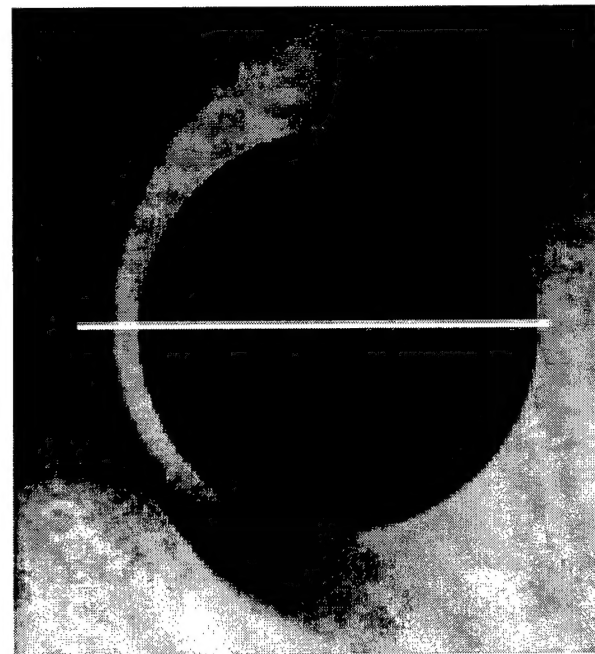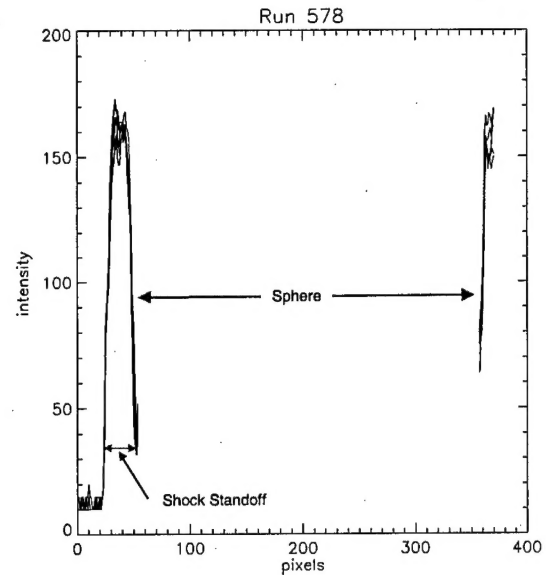
All Data -- A summary of all of the shock standoff data, as derived from the parabolic curve fit procedure, is given in Table 1.

Shock Shape Fit to the Billig Equation

In order to utilize the available measurements of a main portion of the shock shape, shock shape correlation equations developed by Billig[12] were employed. While these correlations would not be expected to apply directly for the weakly ionized plasma, they can be useful for analysis, especially if the primary effect of the weakly ionized plasma is to change the apparent Mach number. The

7

following three equations make up the Billig correlation:

Shock standoff correlation:
$$\delta /R = 0.143 \exp[\, 3.24 / M_\infty^2 \,] \qquad (1)$$
Shock radius of curvature at centerline:
$$R_c / R = 1.143 \exp [\, 0.54 / (M_\infty - 1)^{1.2} \,] \qquad (2)$$
Shock shape:
$$X = R + \delta - R_c \cot^2 \beta \,[(1+(y^2 \tan^2 \beta)/R_c^2)^{0.5} -1] \qquad (3)$$

In this case the quantity β is interpreted as the Mach angle. These correlations were utilized in two ways.
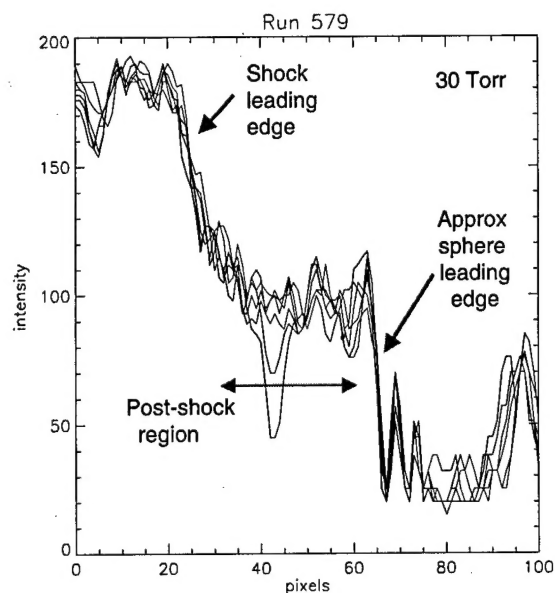

Figure 12. Shock transition analysis (3.1 msec after plasma cut-off).
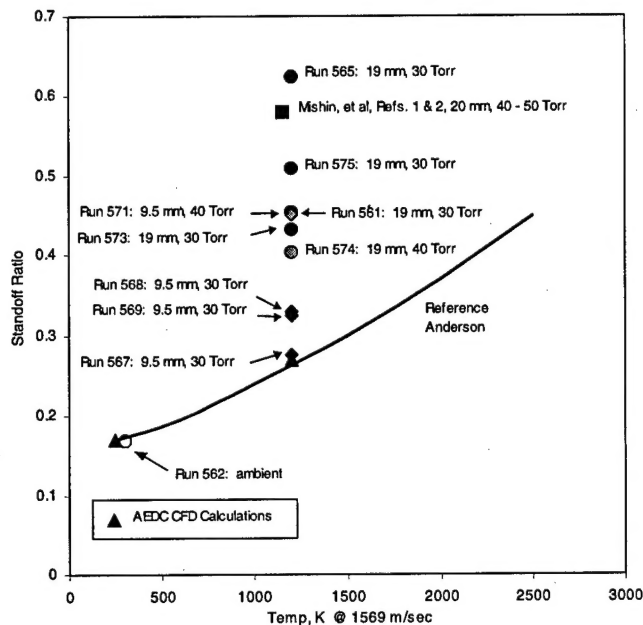

Figure 13. Standoff ratio results.
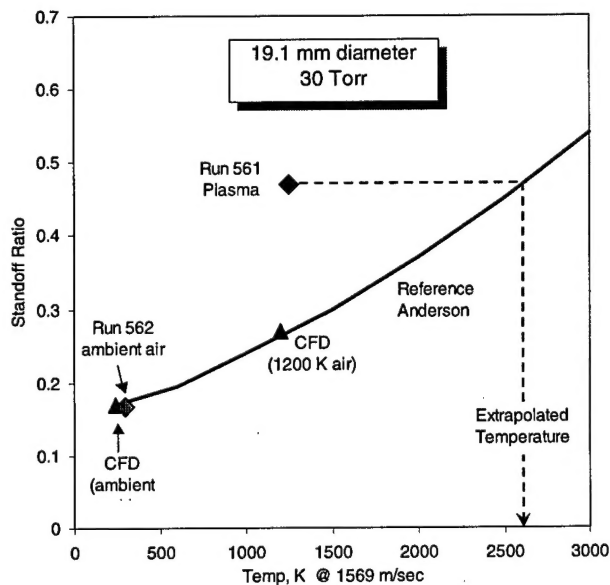
Figure 14. Temperature extrapolation assuming uniform gas temperature.

Recalculation of Shock Standoff -- A best fit of the correlation, Eq. (3), was determined for the entire measured shock shape. An example of this analysis is shown in Fig. 18. Using the Mach number that gave the best fit, the shock standoff distance was calculated from Eq. (1). This approach tacitly assumes a relatively uniform flow field where the same Mach number is used in Eqs. (1) and (2). In some cases, this value was

Figure 15. Shock standoff data summary of plasma cutoff tests.

Figure 16. Comparison of curve fit data to CFD calculations (19-mm sphere)
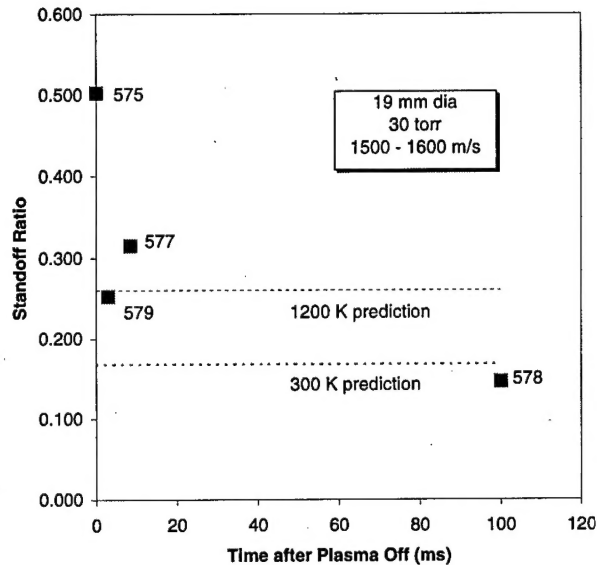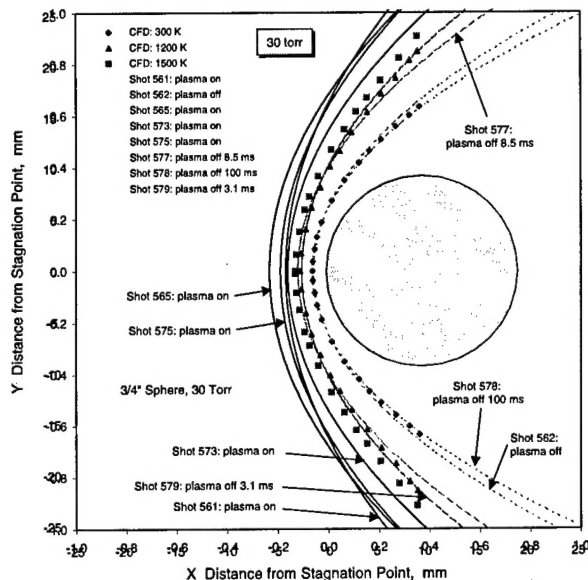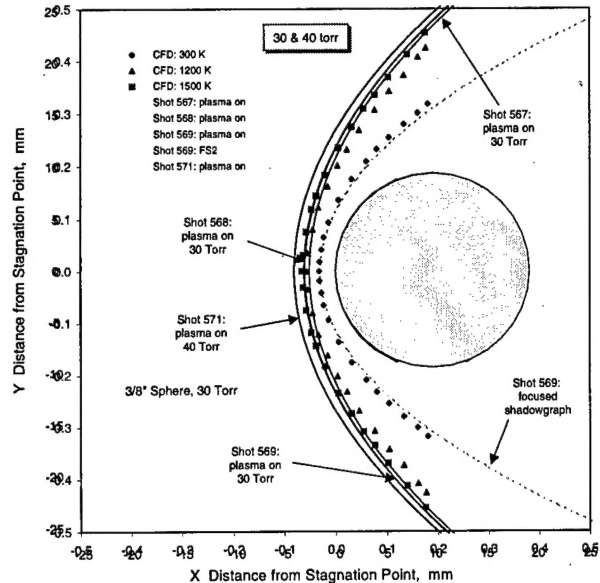

Figure 17. Comparison of curve fit data to CFD calculations (9.5-mm sphere).

standard deviation for the 19.1-mm spheres is 0.017, and 0.028 for the 9.5-mm spheres.

Inference of Temperature -- An effort was also made to use the Billig correlations to assess the nonuniformity of the flow field. This involves a

Shot #	Date	Sphere Dia. (in)	Range Pressure (torr)	Velocity (m/s)	S/R	Plasma Off (ms)
561	6/17/97	0.75	30.3	1597	0.45	
562	6/18/97	0.75	30.3	1647	0.18	
564	6/19/97	0.75	39.9	1558	0.56	
565	7/7/96	0.75	28.3	1562	0.63	
567	7/10/97	0.375	30.4	1630	0.28	
568	8/6/97	0.375	30.1	1599	0.33	
569	8/6/97	0.375	30.7	1578	0.32	
571	8/7/97	0.375	39.8	1604	0.45	
573	11/5/97	0.75	30.5	1516	0.43	
574	11/7/97	0.75	40.3	1521	0.40	
575	11/10/97	0.75	30.1	1588	0.51	
577	11/12/97	0.75	29.9	1502	0.33	8.5
578	11/13/97	0.75	30.2	1498	0.16	100
579	11/14/97	0.75	29.8	1592	0.28	3.1

Table 1. Summary of Standoff Ratio Data

significantly different from the directly measured shock standoff distance. Overall, the scatter in the data is reduced by using these correlations. The 9.5-mm shots exhibit a lower value of shock standoff distance when compared to the 19.1-mm data.

The standard deviation for the measured shock standoff distance, δ/R, was 0.119 for all plasma shots. Using the Billig correlation method reduced it to 0.072. If the shots are grouped by size and only the 30-torr data are considered, the

two Mach number model where the Mach numbers in Eqs. (1) and (2) are allowed to be different. The Mach number in Eq. (1), $M_{\infty 1}$, is assumed representative of the flow near the sphere centerline, while the Mach number in Eq. (2) is assumed to be representative of the far field flow, i.e., out near the shoulder of the sphere. It was found that a very good fit to the plasma shock measurements could be obtained in this manner.

Free-stream Mach numbers can be inferred from the shock standoff distances. The Mach number is the independent variable in the
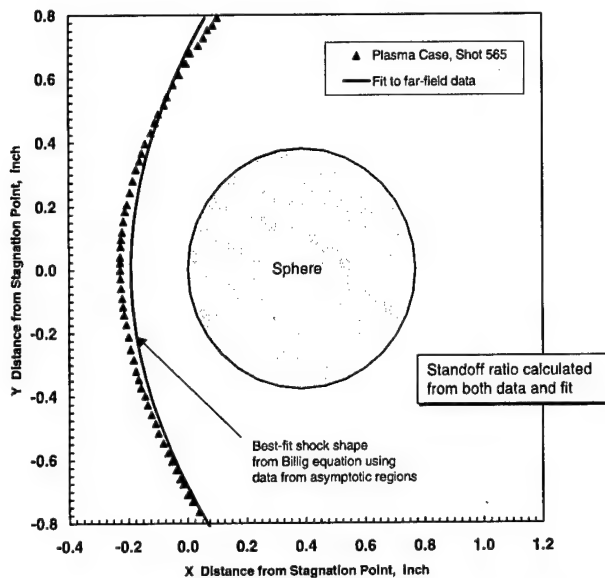
9

Figure 18. Analysis of shock shape using fit to Billig equation.

Figure 19. Inferred temperature from far-field fits showing scale grouping.

correlations and can be computed from Eq. (1) for the direct measurements of shock standoff distance. Because the velocity was measured for each shot, a free-stream temperature required to produce the measured δ can be computed based on the temperature dependence of the sound speed. Again, the data scatter is reduced when the correlations are used. The implied temperature for shots run shortly after the plasma is turned off is considered to be more representative of the measured gas temperatures.

A standard deviation analysis similar to that discussed above was performed on the implied temperatures. In Fig. 19, bands of ($T_{ave} \pm$ standard deviation) are plotted for both the 9.5-mm and the 19.1-mm spheres. The bands are significantly different, indicating that there is a scale effect that is not accounted for by the δ/R nondimensionalization. The ratio of the vertical dimension of the plasma generator to the sphere diameters is approximately 3:1 and 6:1. The curve shown here gives the temperature dependence of the shock standoff and was taken from Ref. 11. The AEDC data fall below the Russian data, especially that derived from the application of the correlations.

Some indication of the temperature nonuniformity in the flow can be obtained by allowing the Mach numbers in Eqs. (1) and (2) to vary independently when fitting the shock shapes as discussed above. Here it is the difference between these temperatures that is significant. This difference seems to disappear after the plasma is turned off.
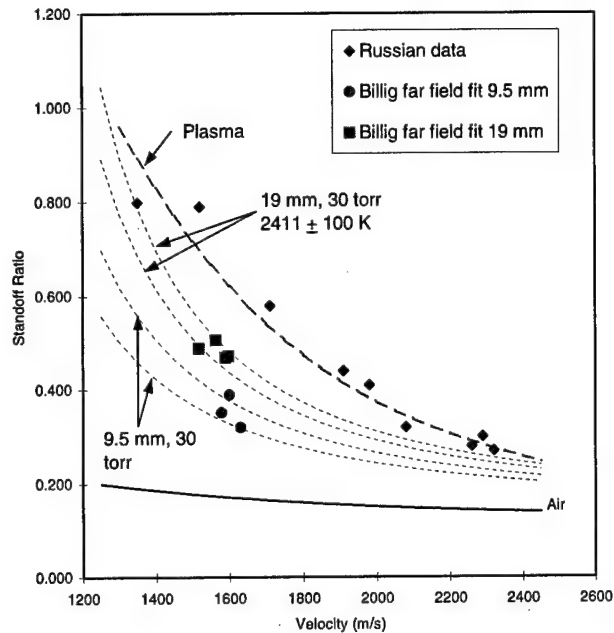
Projectile Location

The holography data were also used to examine the location of the projectile from shot to shot. The reconstruction system was operated in a zoomed-out manner so that the plasma electrodes were contained in the picture. These electrodes gave position reference information so that the position of the sphere for each shot could be determined. A composite of the images of four shots (9.5-mm spheres) is shown in Fig. 20. The maximum differences between the shots in the axial and radial directions are 5.8 and 14.7 mm, respectively. Advances in triggering precision resulted in a very repeatable measurement in axial location, with nontrivial scatter in shot-to-shot height.

Modeling And Simulation

Nonuniform Flow Analysis - CFD Approach

-- It has been shown that temperature gradients in the flow can significantly affect shock wave behavior[13]. A series of CFD solutions was carried out using the TUFF code[14] to assess the effect of a nonuniform temperature distribution in the flow field on the shock shape standing in front of a sphere in supersonic flow. A temperature excess or deficit was assumed to exist in the far field at a distance of 2.4 R_b from the centerline for two cases, a parabolic and a linear dependence. The centerline temperature was held at 1200 K; therefore, the shock standoff distance remained constant for all cases. The CFD results were compared with the Billig correlations using the two
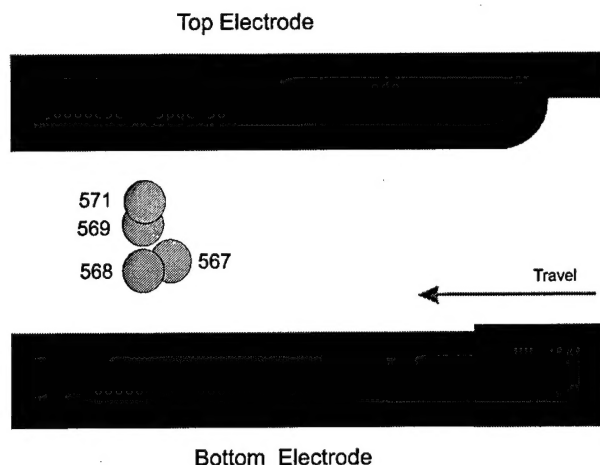
10

Top Electrode

Bottom Electrode

Figure 20. Projectile locations.

Mach number procedure postulated earlier. The CFD solution for a uniform flow temperature of 1200 K and the Billig correlation (also at 1200 K) agree very well. It appears the Billig correlation can be used as a first-order approximation to infer temperature variations as previously discussed. This CFD work is being continued with the objective of producing a more appropriate shock shape correlation in the presence of a nonuniform temperature field.

Shock Tube Analysis — A shock tube problem was selected for a small modeling and simulation effort because it seemed to be a good way to study the basic physics without having to involve multidimensional calculations. A 3-fluid, 1-D model for studying shock propagation in a weakly ionized fluid has been formulated and the describing equations developed. A 3-fluid, 1-D code is under development. The momentum equations contain the collision and electric field terms and are complete except for the viscosity terms. The energy equations still lack the coupling (i.e., collision) terms. Also, in light of the large local electric fields developing in the shock region, it will be necessary to include ionization chemistry. Initial results look promising, and the code appears to be stable. Further work will incorporate the terms mentioned into the code and perform some parameter studies to explore the capabilities of the code and the model.

Uncertainties

The two main data products from this investigation are shock standoff distances and gas temperature. For the shock standoff ratio, estimates can be made on the uncertainties involved in the reading of the hologram, including the quality of the photograph, the width of the shock transition, and the operating conditions (velocity, pressure, and temperature). The chief contribution to the uncertainty, however, is the fluctuating nature of the plasma, both temporally and spatially. Until this is properly mapped and the effects of the variations on the shock standoff ratio are determined, there can be no rigorous determination of the uncertainty in the shock standoff ratio data. The best estimate for the uncertainty is derived from the standard deviations for similar shot conditions and is on the order of ± 20 percent.

In a similar way, although the temperature measurement uncertainty could be characterized by examining the uncertainties due to laser power fluctuations, camera noise, and gate timing, the overwhelming contribution comes from the temporal variation of the plasma. The best estimate for the uncertainty at this stage is ± 20 percent.

Summary

The S1 range facility was configured for shooting projectiles through a weakly ionized gas or plasma. Electrodes were installed and modified to provide the most spatially uniform discharge possible within the scope of the program. The RF generation system used to drive the plasma was modified to duplicate as closely as possible the conditions produced in the Russian tests. Routine operation of this RF generator was established, along with modifications which enabled transient testing. Successful launches were made of 9.5-mm and 19.1-mm diam spheres at 30 and 40 torr at velocities on the order of 1600 m/sec. Holography data showed that the shock shape was indeed altered for projectiles shot through the plasma, thus validating the Russian results. Data were also acquired at various times (3 to 100 msec) after the plasma had been cut off.

A variety of instruments were utilized in addition to the holography. These included an emission camera that was gated to visualize the plasma in coincidence with the projectile arrival; a spectrometer to characterize the excited species in the plasma; a range vibration monitor; a wide FOV emission monitor capable of measuring plasma cut-off transients; and a laser-induced fluorescence (PLIF) system to measure NO rotational temperature.

An extensive effort was made to measure the temperature of the gas in the plasma to aid in discriminating between a thermal-only and an ionization effect. The temperature was measured by three different techniques that gave results as

shown in Fig. 21 of temperatures that were significantly less than those required to explain the shock standoff effect by uniform temperature phenomena alone.

Proposed Future Work

Perhaps the greatest recommendation would be the establishment of a uniform plasma in which to perform the shock standoff tests. The AEDC plasma generator was designed to match the Russian hardware and was not optimized for uniformity. Extensive efforts to produce a uniform
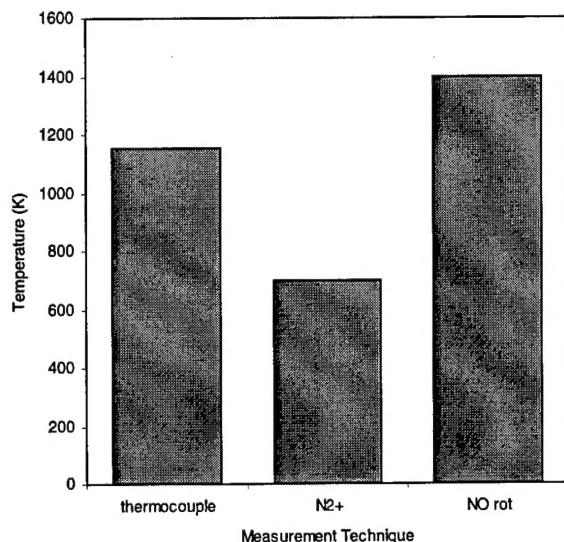

Figure 21. Comparison of temperature results.

plasma from this original setup have not been successful. Though the introduction of a small amount of helium into the range may yield some improvement, the better approach would be the installation of a new generator design. Towards this goal, other plasma generator designs will be considered for installation in the S1 range.

Cooperation and partnering with other centers of expertise will be emphasized as much as possible to determine the type of generator needed. In the meantime, work will continue with the AEDC generator. This could include a series of shots where the projectile is captured in different areas of the structure of the plasma, and a series with the plasma current and/or voltage at different levels to address the significance of the electronic properties of the plasma.

The capability of turning the plasma on very quickly, so that the plasma region can be investigated before the gas temperature rises

significantly, is preferred to the existing quick turn-off system. It may be that plasma initiation by photonic means, or the use of a pulsed e-beam for plasma generation, will be well suited to the range. These options will be assessed for their operational utility.

The characterization of the plasma is very important to the proper understanding of the flow-field environment. The installation of an existing microwave interferometer (31 GHz) to make measurements of electron temperature and density is planned. Further work on the temperature probe will continue, and surface conductivity probes developed by AFRL will be investigated.

Shots are planned in other gases instead of air, as this could yield important information concerning the physical mechanisms behind the shock standoff effect. Two easily adaptable possibilities are dry nitrogen and argon. Argon, in particular, presents a very different type of medium: a monatomic inert gas with no vibrational or rotational modes for which the γ would not change in the plasma.

The measurement of gas temperature remains an important issue. Though the measurement of gas temperature in argon is very difficult, nitrogen runs hotter, and a measurement of its temperature can be used for the upper limit of the argon temperature. Measurements will thus be made for different mixtures of nitrogen and argon and an extrapolation made to the pure argon case. The measurement of N_2 and/or N_2^+ spectra will be used to make this temperature determination. The NO-PLIF temperature measurement technique will be continued so that temperature mapping in the plasma with respect to the vertical direction can be accomplished.

The analysis and modeling efforts will be continued and expanded. A more detailed examination of the experimental scatter will be performed, possibly with further shots for statistical purposes. Emphasis will be on the variance in the holographic playback part of the data reduction process. The analysis of the shock shape through the Billig equations will also be continued, along with further examination of the effect of temperature variations and gradients through CFD modeling. A measurement uncertainty analysis will also be performed for the NO-PLIF temperature technique. Further modeling of the radiative emission and analysis of spectral data is planned.

Improvements in the holography system beyond those which have already been

accomplished will be pursued, including the minimization of atmospheric disturbances and the use of a higher power laser to improve the throughput. In addition, work on a novel, controlled "dynamic-playback" of holograms which quantifies phase (density) changes across the aerodynamic shocks will continue. The use of a better, possibly a CCD, camera is also being considered for immediate image digitization. Further development will be directed at improving the stability of the playback optics setup to minimize vibration-induced noise, and developing the plate-shifting hardware for smooth operation.

For high-speed flow visualization, a copper-vapor laser and drum camera recently acquired by the AEDC could be configured to provide the several images of the shock structure as the projectile passes through the plasma region. This laser can achieve 50-kHz operation, which would yield an image approximately every 3 cm. A movie of such plasma dynamics would yield important information about the temporal characteristics of the plasma (possible generation of plasmoids and other structures). The data obtained would provide an indication of how steady the plasma is during a shot and reveal how accurately the pre-shot plasma characterization reflect the actual conditions during a shot. An Air Force-funded SBIR, could in the near future, provide the capability for holographic recording with this system.

The possibility of introducing an erosive plasma generator in scale models for testing in various other AEDC facilities such as Tunnel A, APTU, or 16T is being pursued. Also, a wide-angle cone with a spherical tip has been designed as a projectile for possible use with regard to enhancing the strength of the shock.

The modification of the test section of an existing, operational, laboratory shock tube to accommodate "plasma effect" experiments is being studied. The system will be constructed such that the plasma discharge could remain on, or be turned off just before the arrival of the flow at the model. The plasma would be a DC discharge created using ring electrodes, similar to the discharge region of a CO_2 laser, without mirrors. Existing diagnostics would be used to monitor flow conditions. This capability would provide the experimental database required for CFD modeling.

REFERENCES

1. Lowry, H.S., et al. "Characterization of the Shock Structure of a Spherical Projectile in Weakly Ionized Air through Ballistic Range Test Techniques." 2nd Weakly Ionized Gases Workshop, Norfolk VA, April 24-25, 1998.

2. Blanks, James R. and Lowry, Heard S. "Supersonic Projectile Tests in a Weak Plasma." AEDC-TR-98-1, October 1998.

3. Mishin, G. I., Serov, Yu. L., and Yavor, I. P. "Flow Around a Sphere Moving Supersonically in a Gas Discharge Plasma." Pis'ma Zh. Tekh. Fiz. (Soviet Technical Physics Letters) 17, June 12, 1991, pp. 65-71.

4. Bedin, A. P. and Mishin, G. I. "Ballistic Studies of the Aerodynamic Drag on a Sphere in Ionized Air." Pis'ma Zh. Tekh. Fiz. 21, January 12, 1995, pp. 14-19.

5. Hiden Analytical Limited. Handbook of Plasma Diagnostics. 420 Europa Boulevard, Warrington WA5 SUN, England.

6. Gochberg, L.A. "The Electron Beam Fluorescence Technique in Hypersonic Aerothermodynamics." AIAA-94-2635, 18th Aerospace Ground Testing Conference, Colorado Springs, CO, June 20-23, 1994.

7. McMillin, B. K., Palmer, J. L., and Hanson, R. K. "Temporally Resolved, Two Line Fluorescence Imaging of NO Temperature in a Transverse Jet in a Supersonic Cross Flow." Applied Optics, Vol. 32, No. 36, December 20,1993, pp. 7532-7545.

8. Cassady, P. E. and Lieberg, S. F. "Planar Laser Induced Fluorescence of NO (A-X) in Hypersonic Flowfields." AIM Paper 92-2962, AIM 23rd Plasmadynamics and Lasers Conference, Nashville, TN, July 6-8,1992.

9. Ruyten, W.M., Smith, M.S., Price, L.L., and Williams, W.D. "Three-Line Flourescence Thermometry of Optically Thick Shock-Tunnel

Flow." Applied Optics, Vol. 37, No. 12, April 20, 1998, pp. 2334-2339.

10. Ruyten, W.M. "Comparison of Calculated and Measured Temperature Fields in the AEDC Impulse Facility." AIAA Paper 96-2237, New Orleans, LA, June 1996.

11. Anderson, J.D. Hypersonic and High Temperature Gas Dynamics, McGraw-Hill, 1989, New York, pp. 189-192.

12. Billig, F.S. "Shock-Wave Shapes Around Spherical- and Cylindrical-Nosed Bodies."

Journal of Spacecraft and Rockets, Vol. 4, No. 6, June 1967, pp. 822-823.

13. Hilbun, William M. "Shock Waves in Non-equilibrium Gases and Plasmas." PhD Thesis, Air Force Institute of Technology, October 1997.

14. Molvik, G.A. and Merkle, C.L. "A Set of Strongly Coupled, Upwind Algorithms for Computing Flows in Chemical Nonequilibrium." AIAA Paper 89-0199, January 1989.